

## Quantum Logic Enhanced Sensing in Solid-State Spin Ensembles

Nithya Arunkumar,<sup>1,2,3</sup> Kevin S. Olsson<sup>3,4,5</sup> , Jner Tzern Oon<sup>3,6</sup> , Connor A. Hart,<sup>3,4</sup> Dominik B. Bucher,<sup>1,7</sup> David R. Glenn,<sup>1</sup> Mikhail D. Lukin,<sup>1</sup> Hongkun Park<sup>1,8</sup> , Donhee Ham,<sup>2</sup> and Ronald L. Walsworth<sup>1,3,4,6,\*</sup>

<sup>1</sup>Department of Physics, Harvard University, Cambridge, Massachusetts 02138, USA

<sup>2</sup>John A. Paulson School of Engineering and Applied Sciences, Harvard University, Cambridge, Massachusetts 02138, USA

<sup>3</sup>Quantum Technology Center, University of Maryland, College Park, Maryland 20742, USA

<sup>4</sup>Department of Electrical and Computer Engineering, University of Maryland, College Park, Maryland 20742, USA

<sup>5</sup>Intelligence Community Postdoctoral Research Fellowship Program, University of Maryland, College Park, Maryland 20742, USA

<sup>6</sup>Department of Physics, University of Maryland, College Park, Maryland 20742, USA

<sup>7</sup>Department of Chemistry, Technical University of Munich, Lichtenbergstraße 4, 85748 Garching, Germany

<sup>8</sup>Department of Chemistry and Chemical Biology, Harvard University, Cambridge, Massachusetts 02138, USA

 (Received 8 May 2022; revised 11 May 2023; accepted 15 May 2023; published 5 September 2023)

We demonstrate quantum logic enhanced sensitivity for a macroscopic ensemble of solid-state, hybrid two-qubit sensors. We achieve over a factor of 30 improvement in the single-shot signal-to-noise ratio, translating to an ac magnetic field sensitivity enhancement exceeding an order of magnitude for time-averaged measurements. Using the electronic spins of nitrogen vacancy (NV) centers in diamond as sensors, we leverage the on-site nitrogen nuclear spins of the NV centers as memory qubits, in combination with homogeneous and stable bias and control fields, ensuring that all of the  $\sim 10^9$  two-qubit sensors are sufficiently identical to permit global control of the NV ensemble spin states. We find quantum logic sensitivity enhancement for multiple measurement protocols with varying optimal sensing intervals, including XY8 and DROID-60 dynamical decoupling, as well as correlation spectroscopy, using an applied ac magnetic field signal. The results are independent of the nature of the target signal and broadly applicable to measurements using NV centers and other solid-state spin ensembles. This work provides a benchmark for macroscopic ensembles of quantum sensors that employ quantum logic or quantum error correction algorithms for enhanced sensitivity.

DOI: [10.1103/PhysRevLett.131.100801](https://doi.org/10.1103/PhysRevLett.131.100801)

Quantum technologies for information processing, networking, and sensing increasingly employ hybrid architectures leveraging the advantageous properties of multiple physical qubit types. In platforms for quantum computing, this approach enables increased system sizes, while maintaining high fidelity and low crosstalk [1–4]. For time-keeping applications, ion clocks using two species, one “clock” ion with a stable transition and a second “logic” ion for preparation and readout, have demonstrated exceptional performance [5–8].

Analogous multiqubit strategies are similarly compelling for quantum sensors. In particular, the use of additional memory qubits in support of sensing qubits presents an attractive avenue towards entanglement-enhanced performance using quantum logic [9,10]. Among leading quantum sensing platforms, defect centers in solid-state systems are naturally amenable to quantum logic assisted protocols since they commonly consist of multiple individually controllable spin degrees of freedom localized within or near a defect.

An early demonstration of such multiqubit sensing by Jiang *et al.* used a single-negatively charged nitrogen-vacancy (NV) center spin state coupled to a nearby  $^{13}\text{C}$

nuclear spin [11]. The technique overcomes the poor optical readout fidelity of NV centers by using quantum logic to map the NV electronic spin state onto the longer-lived  $^{13}\text{C}$  nuclear spin memory qubit. This protocol repeatedly interrogates the  $^{13}\text{C}$  spin by reentangling it with the NV electronic spin between each optical readout.

Subsequent work with single NV centers improved upon this protocol by instead using the nitrogen nuclear spin inherent to the NV center as a memory qubit [12,13]. In contrast to the randomly distributed  $^{13}\text{C}$  nuclear spins, the on-site nitrogen nuclear spin has a well-determined hyperfine coupling with the NV electronic spin. This homogeneous coupling makes it particularly suitable for translation to ensembles of NV centers, as reported here.

NV ensemble measurements trade nanometer-scale spatial resolution for dramatically improved sensitivity [9], enabling a wide range of applications across the physical and life sciences, including micron-scale nuclear magnetic resonance (NMR) [14], magnetic microscopy [15], crystal stress and pressure spectroscopy [16,17], and thermometry [18,19]. However in nearly all such experiments, only global control of the NV ensemble is available. Therefore, the useful realization of quantum logic protocols with NV

ensembles demands each constituent multiqubit sensor system be nearly identical, for both interactions within the NV center and diamond lattice, as well as in response to external fields.

In this Letter, we demonstrate quantum logic enhanced (QLE) sensing with a macroscopic ensemble of two-qubit sensors, each consisting of a NV electronic spin and its on-site  $^{15}\text{N}$  nuclear spin. Interrogating a  $2.3 \times 10^3 \mu\text{m}^3$  volume of diamond containing  $\sim 10^9$  of these two-qubit sensors, with careful control of ensemble homogeneity and stability, the QLE protocol increases the effective readout fidelity of each constituent NV, achieving a  $33\times$  improvement in single shot signal-to-noise ratio (SNR) compared to measurements using only the NV electronic spins (i.e., with conventional NV readout). This observed SNR improvement translates to enhancements in ac magnetic field sensitivity for repeated (i.e., time-averaged) measurements that can exceed an order-of-magnitude over conventional, non-QLE readout. Importantly, the present approach is universally applicable (independent of the sensing protocol or target signal), and thus provides a benchmark for quantum sensing using quantum logic architectures, both for ensembles of NV centers and other platforms.

Figure 1(a) illustrates the experimental setup (further detail the in Supplemental Material [20]), which operates at ambient laboratory conditions and probes a  $(2 \times 2 \times 0.5) \text{ mm}^3$  diamond chip. In this chip, a  $13 \mu\text{m}$  layer contains an ensemble of NV centers at a concentration of  $[\text{NV}] \approx 2.3 \text{ ppm}$  ( $[\text{N}] \approx 14 \text{ ppm}$ ) [21]. Each near-identical two-qubit system in the ensemble consists of the NV electronic “sensor” spin ( $S = 1$ ) and the nuclear “memory” spin ( $I = 1/2$ ) of the associated  $^{15}\text{N}$  nucleus. By applying a bias magnetic field along an NV symmetry axis, the NV ground state spin sublevels are nondegenerate [Fig. 1(b)], allowing them to be individually addressed using microwave fields. We employ the NV electronic spin states  $m_s = 0$  and  $m_s = -1$  as an effective two-level system, with representative qubit states  $|\downarrow_e\rangle$  and  $|\uparrow_e\rangle$ , respectively. The two NV nuclear spin states  $m_I = -\frac{1}{2}, \frac{1}{2}$  are represented by  $|\downarrow_n\rangle$  and  $|\uparrow_n\rangle$  qubit states. The eigenstates of the composite electronic-nuclear system are denoted by  $\{|\uparrow_e, \downarrow_n\rangle; \{\uparrow_n, \downarrow_n\}\}$ .

We first demonstrate control of the NV nuclear spin (memory qubit) using the NV electronic spin (sensor qubit) via a quantum logic protocol. Figures 2(a) and 2(c) illustrate this procedure, which begins with a selective microwave (MW)  $\pi$  pulse that exchanges the spin populations of the states  $|\downarrow_e; \uparrow_n\rangle$  and  $|\uparrow_e; \uparrow_n\rangle$ . This pulse acts as a CNOT operation on the electronic spin, conditioned on the nuclear spin state (CNOT $_{e|n}$ ). Next, a radio frequency (rf)  $\pi$  pulse is applied, resulting in a CNOT $_{n|e}$  gate that exchanges the populations of  $|\uparrow_e; \uparrow_n\rangle$  and  $|\uparrow_e; \downarrow_n\rangle$ . This operation encodes the information measured by the sensor spins onto the memory spins. These two CNOT gates, applied in succession, form a SWAP operation (i.e., gate) of duration  $T_{\text{SWAP}}$ .

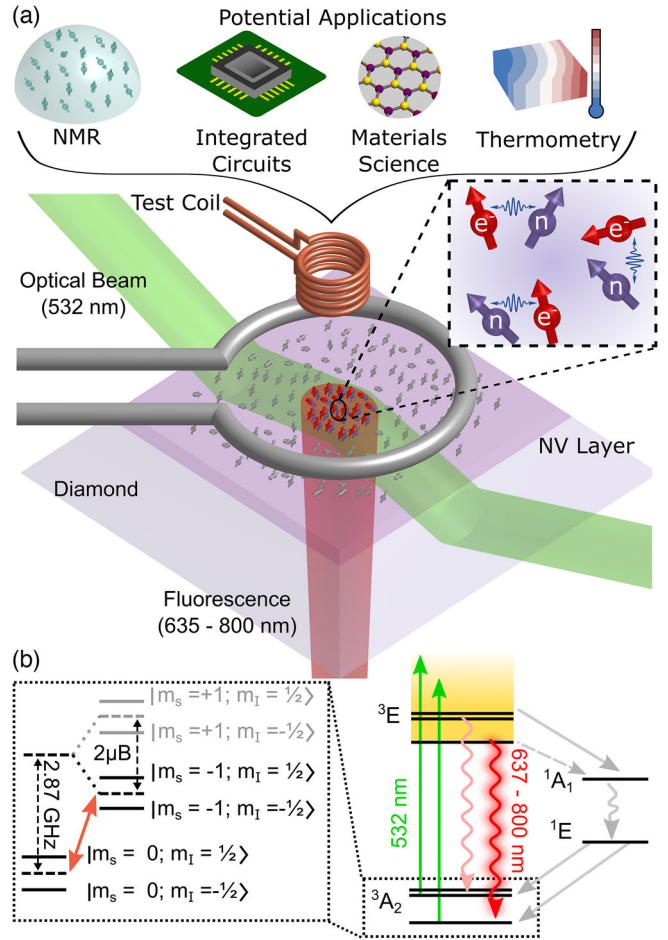


FIG. 1. NV ensemble sensor integrated with quantum logic. (a) A 532 nm optical beam enters the diamond chip through its side (45° angle cut), using total internal reflection to illuminate a spot diameter of  $\sim 15 \mu\text{m}$  on the top surface of the diamond chip, where the  $13 \mu\text{m}$  thick NV layer resides. A 1 mm diameter, single-loop antenna at  $\sim 0.5 \text{ mm}$  above the NV layer drives both the microwave transition of the NV electronic spin states and the radio frequency transition of the  $^{15}\text{N}$  nuclear spins [20]. The magnified view depicts the multi-qubit NV spin sensors comprising an ensemble of  $\sim 10^9$  NVs in the detection region. A multiloop test coil provides the synthetic ac magnetic field measured in this study, emulating those originating from, e.g., NMR, integrated circuits, materials science, and thermometry applications. (b) NV energy levels allow optical initialization and readout of the electronic spin states, with splitting of the ground state triplet energy levels from Zeeman and hyperfine interactions.

The fidelity of the CNOT gates is limited by the spin transition linewidths, with contributions from both the intrinsic linewidth of the NV ensemble  $\delta\nu \sim 1/\pi T_2^*$  and dephasing from inhomogeneities in the bias and control fields across the interrogation volume [9]. Here, the external inhomogeneities over the ensemble are  $\sim 0.2 \text{ kHz}$  for the bias field,  $\sim 10 \text{ kHz}$  for the lattice strain, and  $\sim 4\%$  in the applied MW and rf control fields [20].

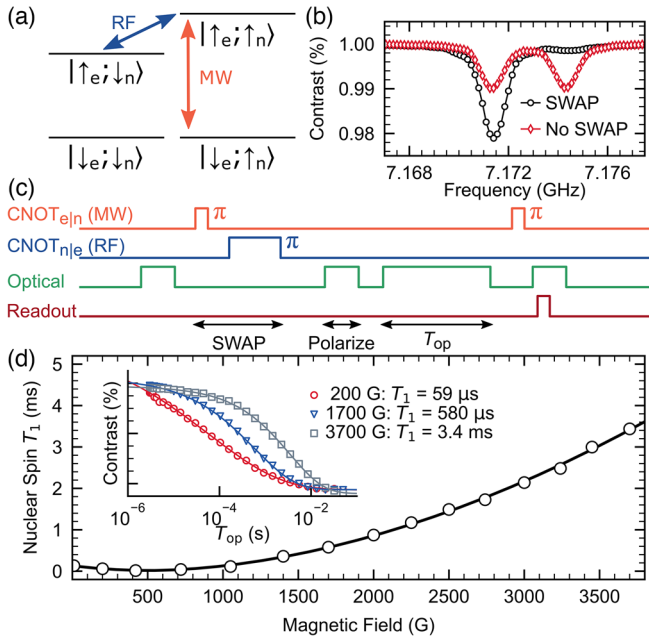


FIG. 2. Nuclear spin control with quantum logic. (a) Energy levels of the two-qubit system are shown for the NV electronic spin states ( $\{|\uparrow_e, \downarrow_e\rangle\}$ ) and its on-site  $^{15}\text{N}$  nuclear spin states ( $\{|\uparrow_n, \downarrow_n\rangle\}$ ). Microwave (MW) and radiofrequency (rf) pulses act as  $\text{CNOT}_{e|n}$  and  $\text{CNOT}_{n|e}$  gates, respectively. Applying these gates in succession constitutes a SWAP operation. (b) Measured NV ensemble ODMR spectra with and without the SWAP operation. (c) Experimental pulse sequence used to measure the nuclear spin lifetime  $T_1$  under optical illumination of variable duration  $T_{op}$ . (d) Measured bias magnetic field dependence of  $^{15}\text{N}$  ensemble nuclear spin lifetime  $T_1$ , under 130 mW of optical illumination power (used for all measurements in the main text), fit to a power law. Inset: Examples of data used for extracting  $T_1$  values. Minimum  $T_1$  is near the excited state level anticrossing of field  $\sim 500$  G. See Supplemental Material for full data [20].

Thus, the CNOT gate fidelities used here are limited by the intrinsic broadening, with linewidth  $\delta\nu \approx 0.5$  MHz ( $T_2^* = 600$  ns). With this linewidth limited broadening, the estimated fidelity of spin population transfer by the SWAP operation  $\approx 93\%$ , as shown in Fig. 2(b).

After encoding the sensor spin population onto the memory spins using the SWAP gate, the electronic spin states are reset using an optical polarization pulse. With successive  $N$  applications of an entangling  $\text{CNOT}_{e|n}$  gate followed by an optical readout pulse, the information stored in the nuclear memory spins is then repeatedly mapped back onto the electronic spins and measured optically. This procedure provides many readouts within a duration limited by the nuclear spin lifetime  $T_1$ , thereby enhancing the overall readout fidelity. The large number of NVs probed allows a high-precision, ensemble-averaged measurement of the sensor spin state with one execution of this repeated readout procedure.

The nuclear spin  $T_1$  increases with external bias magnetic field due to suppression of flip-flop transitions of the

electronic and nuclear spins. We measure  $T_1$  using the pulse sequence in Fig. 2(c) for magnetic fields up to 3700 G, see Fig. 2(d). The inset of Fig. 2(d) shows example  $T_1$  values extracted from fits of the NV ensemble fluorescence contrast to  $a * \exp[-(T_{op}/T_1)^c] + d$ . The  $T_1$  values follow the expected quadratic dependence on magnetic field due to anisotropic hyperfine spin state mixing [12]. Full magnetic field and laser power dependent  $T_1$  measurements are shown in the Supplemental Material [20]. The following measurements use a bias magnetic field of 3700 G, with a corresponding  $^{15}\text{N}$  nuclear spin  $T_1$  of 3.44(12) ms.

We demonstrate quantum logic enhanced (QLE) ac magnetic field sensing by measuring a three-tone test signal centered at 1 MHz, applied to the NV ensemble via a multiloop coil (see Fig. 1, and Supplemental Material [20]). First we use correlation spectroscopy, a popular NV  $T_1$ -limited technique for ac magnetometry, where the time delay between two dynamical decoupling sequences ( $T_{corr}$ ) is varied, see Fig. 3, with optical readout applied only after the second decoupling sequence [33–38]. Our correlation spectroscopy measurement employs the dynamical decoupling sequence XY8:6 (six repetitions of an XY8 sequence) [39,40]. As shown in Fig. 3, the sensing interval  $T_{sense}$  is followed by a SWAP operation and optical reinitialization pulse (with overall duration  $T_{SWAP}$ ) and  $N$  quantum logic readout (QLR) cycles (each with duration  $T_{QLR}$ ). The

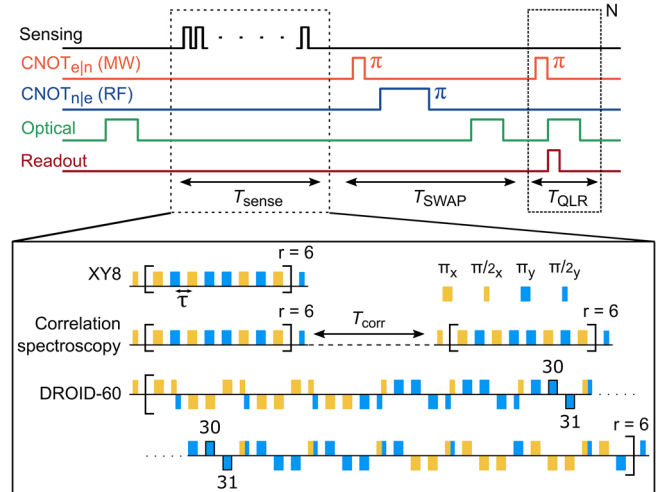


FIG. 3. Quantum logic enhanced (QLE) sensing protocol. After a sensing sequence with duration  $T_{sense}$ , the electronic spin state is encoded onto the nuclear spin for each NV in the ensemble via application of  $\text{CNOT}_{e|n}$  and  $\text{CNOT}_{n|e}$  gates, forming a SWAP operation of duration  $T_{SWAP}$ , including an optical pulse that repolarizes the electronic spins. The readout sequence, consisting of a  $\text{CNOT}_{e|n}$  gate and a repolarization pulse, is then repeated  $N$  times. The duration of each individual quantum logic readout sequence,  $T_{QLR}$ , is limited by the time required to repolarize the electronic spins. Example ac magnetic field sensing sequences are shown in the magnified view of  $T_{sense}$ .

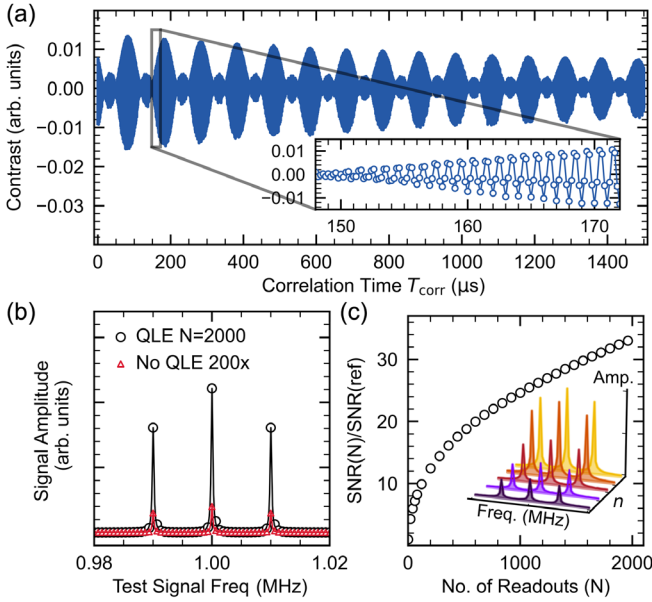


FIG. 4. Quantum logic enhanced (QLE) readout demonstrated with correlation spectroscopy. (a) Example measured NV correlation spectroscopy time trace for the three-tone test signal, without the QLE protocol. (b) Power spectra of the correlation spectroscopy signal with and without the QLE protocol. The power spectrum in the absence of quantum logic is scaled by 200 $\times$  for visibility. (c) Signal-to-noise ratio of the measured test signal as a function of the number of quantum logic readout (QLR) cycles,  $N$ , compared to the reference SNR of a single readout sequence without the QLE protocol. Inset shows the decreasing signal amplitude from conventional readout (lightest) compared to the  $n$ th QLR cycle, with  $n = 1, 600, 1300$ , and 2000 (darkest), due to  $^{15}\text{N}$  nuclear spin  $T_1$  relaxation.

correlation spectroscopy signal using the conventional readout method (i.e., single readout per  $T_{\text{corr}}$ ), see Fig. 4(a), yields three well-resolved tones in its power spectrum, shown in Fig. 4(b) and scaled up by a factor of 200.

Applying the QLE sensing protocol to measurements of the three-tone test signal, we determine a series of power spectra from the correlation time series acquired for each of the  $N$  readout cycles. As apparent in the inset of Fig. 4(c), the power spectrum signal amplitudes,  $A_n$ , decay with increasing readout cycle index  $n$  due to  $^{15}\text{N}$  nuclear spin  $T_1$  relaxation. To optimize the signal-to-noise ratio  $\text{SNR}(N)$  after  $N$  readouts [11], the signal amplitude for the  $n$ th readout is weighted by  $A_n/\sigma_n^2$ , where  $\sigma_n$  is the standard deviation of the noise at the  $n$ th readout. Figure 4(b) compares the power spectrum of a weighted signal, after  $N = 2000$  QLR cycles, to the reference signal obtained using conventional readout.

The resulting QLE signal to noise ratio  $\text{SNR}(N)$  is given by  $\sqrt{\sum_{n=1}^N A_n^2/\sigma_n^2}$ . We normalize  $\text{SNR}(N)$  by  $\text{SNR}(\text{Ref})$ , the SNR of conventional NV electronic spin readout (i.e., single readout), measured under the same experimental conditions. The increase in SNR realized with quantum logic is shown in Fig. 4(c). For example, with 2000 QLR cycles, we increase

the SNR by 33.3(9) $\times$ , larger than the best value ( $\sim 20\times$ ) previously reported for QLR applied to a single NV [13]. Similar SNR increases with the QLE protocol are found for the other ac magnetic field sensing sequences used in this study (see the Supplemental Material [20]).

However, improvements in SNR do not necessarily translate into enhanced sensitivity, since SNR does not consider the impact on the measurement timescale (and hence bandwidth) of an extended readout interval. Accounting for the overhead time associated with the SWAP operation ( $T_{\text{SWAP}} = 20 \mu\text{s}$ ) and each readout cycle ( $T_{\text{QLR}} = 3 \mu\text{s}$ ), the sensitivity enhancement obtained using the QLE protocol can be estimated using

$$\tilde{\eta}_{\text{QLE}} \approx \frac{\text{SNR}(N)}{\text{SNR}(\text{Ref})} \frac{\sqrt{T_{\text{sense}} + T_{\text{QLR}}}}{\sqrt{T_{\text{sense}} + T_{\text{SWAP}} + (N \times T_{\text{QLR}})}}, \quad (1)$$

where we have assumed the duration of a conventional readout is approximately  $T_{\text{QLR}}$ .

As shown in Fig. 5(a) for an XY8:6 dynamical decoupling sequence with an optimal  $T_{\text{sense}} = 24 \mu\text{s}$ , the quantum logic protocol achieves a sensitivity enhancement of up to  $\tilde{\eta}_{\text{QLE}} = 2.4(3)$  for  $N \approx 150$ , compared to the same sensing sequence with conventional readout. For the diamond sample used here, the optimal  $T_{\text{sense}}$  under XY8 decoupling is constrained by the NV electronic spin XY8 coherence time  $T_2 \approx 31 \mu\text{s}$ , which, in turn, is limited by NV-NV dipolar interactions. The resulting non-QLE ac sensitivity was measured to be 34(1) pT/ $\sqrt{\text{Hz}}$  [20].

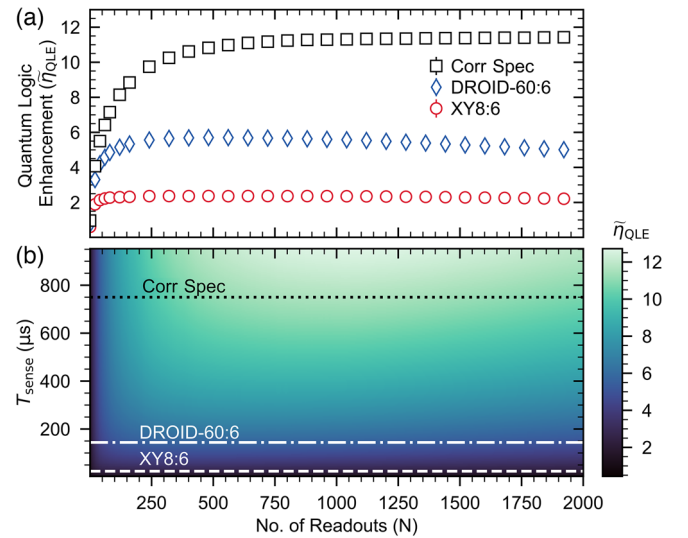


FIG. 5. Quantum logic enhanced (QLE) sensitivity. (a) Experimentally determined QLE sensitivity factor ( $\tilde{\eta}_{\text{QLE}}$ ) as a function of the number  $N$  of quantum logic readouts, for the three types of sensing sequences used in the present work. (b) Calculated  $\tilde{\eta}_{\text{QLE}}$ , given by color bar, as a function of the number of readouts  $N$  and sensing duration  $T_{\text{sense}}$ . Calculations use Eq. (1) and the conditions of the present experiment. Dashed lines indicate the  $T_{\text{sense}}$  values of the three sensing measurements reported in (a).

To surpass the coherence time limit from NV-NV interactions, we employ the DROID-60 decoupling sequence introduced in Refs. [22,23] and thereby extend the optimal  $T_{\text{sense}}$  to about 144  $\mu\text{s}$  [20]. Using DROID-60 with this  $T_{\text{sense}}$ , we measure a non-QLE ac sensitivity of 19.6(8) pT/ $\sqrt{\text{Hz}}$ , comparable to other state of the art ac sensitivities with NV ensembles, e.g., 10.8 pT/ $\sqrt{\text{Hz}}$  [24] and 14.4 pT/ $\sqrt{\text{Hz}}$  [25]; and providing more than an order-of-magnitude better volume-normalized non-QLE ac sensitivity than these other works. See Ref. [20] for further sensitivity discussion. Applying the QLE protocol and comparing it to conventional readout, we find  $\tilde{\eta}_{\text{QLE}} = 5.7(3)$  for DROID-60:6 at  $N \approx 1400$ , as shown in Fig. 5(a). With this enhancement factor, our calculated QLE ac sensitivity is 3.4(1) pT/ $\sqrt{\text{Hz}}$ .

For ac magnetometry using correlation spectroscopy,  $T_{\text{sense}}$  varies with  $T_{\text{corr}}$ . To account for this variation, we compare measurements using quantum logic with  $N$  readouts to conventional measurements repeated  $M$  times, maintaining a constant total acquisition time:  $T_{\text{sense}} + T_{\text{SWAP}} + (N \times T_{\text{QLR}}) = M \times (T_{\text{sense}} + T_{\text{QLR}})$ . For measurements with  $T_{\text{corr}}$  ranging from 0–1.5 ms, we find up to  $\tilde{\eta}_{\text{QLE}} = 11.3(3)$  for  $N \approx 1000$  and above. More intuitively, if we use the average value of  $T_{\text{corr}}$  (0.75 ms) when calculating  $\tilde{\eta}_{\text{QLE}}$  via Eq. (1), we estimate a similar QLE sensitivity factor of  $\tilde{\eta}_{\text{QLE}} \approx 11$ . Finally for correlation spectroscopy, ac sensitivities using  $N = 2000$  QLR cycles were measured to be 47(1) pT/ $\sqrt{\text{Hz}}$  with no QLE, and 4.2(1) pT/ $\sqrt{\text{Hz}}$  with QLE, again yielding a quantum logic enhancement of  $\sim 11$ .

To highlight the versatility of the QLE technique, Fig. 5(b) provides estimates of quantum logic enhancement for a range of sensing durations  $T_{\text{sense}}$ , given our experimental conditions. For moderate nuclear spin lifetimes ( $\sim T_1 > 100 \mu\text{s}$ ), an improvement in sensitivity (i.e.,  $\tilde{\eta}_{\text{QLE}} > 1$ ) is readily achieved when both  $T_{\text{sense}}$  exceeds  $T_{\text{SWAP}}$ , and  $T_{\text{SWAP}}$  is much larger than  $T_{\text{QLR}}$ . These conditions for  $T_{\text{QLR}}$  and  $T_{\text{SWAP}}$  are, respectively, obtained with typical optical intensities  $\sim 0.1$ – $1.0 \text{ mW}/\mu\text{m}^2$  and with commercially available rf amplifiers [20]. Thus, the QLE protocol should be applicable to a wide range of sensing sequences (and diamond materials) commonly used in NV ensemble measurements and, in principle, for other solid-state spin systems.

In summary, we leveraged quantum logic using a macroscopic ensemble of solid-state, hybrid two-qubit sensors—each consisting of an NV electronic spin and on-site  $^{15}\text{N}$  nuclear spin in diamond—to realize a factor of about 30 improvement in spin state readout SNR, which in turn enables significant improvement in ac magnetic field sensitivity. The observed sensitivity enhancements can exceed an order of magnitude under favorable conditions (i.e, sensing interval  $\sim 1$  ms) using only global control of the NV ensemble.

Furthermore, the current approach is agnostic to the target signal and, therefore, broadly applicable to sensing a

variety of physical quantities. In particular, QLE sensing benefits from a strong, uniform bias magnetic field, making the technique well suited for use in NV-NMR spectroscopy [14]. We expect existing NV-NMR systems can readily implement the QLE protocol. Additionally, the sensitivity improvements realized here are compatible with the growing collection of techniques for NV-NMR sample hyperpolarization [26,27].

Beyond magnetometry, NV-diamond dynamical decoupling protocols sensitive to crystal stress, pressure, and temperature have attained sensing durations of tens of microseconds or longer. For example, such sequences were recently employed in path-finding experiments for diamond-based dark matter searches [16]. With further development, the key metric of  $T_{\text{sense}} > T_{\text{SWAP}}$  may be realized for these alternative sensing applications, enabling quantum logic enhanced sensitivity.

Integrating additional quantum degrees of freedom, e.g., defects with couplings to multiple nuclear spins, is another promising direction for further progress in QLE sensing [41–44]. Similarly, solutions to address the random distribution of host lattice nuclear spins, such as manipulating the collective modes of a spin bath [45], may prove advantageous when exploring more advanced quantum logic or error correction algorithms [46] for further sensing enhancements.

This work was supported by, or in part by, the U.S. Army Research Laboratory under Grant No. W911NF1510548; the U.S. Army Research Office under Grant No. W911NF1920181; the Moore Foundation; the DARPA DRINQS program under Grant No. D18AC00033; and the University of Maryland Quantum Technology Center. D. B. B. was partially supported by the German Research Foundation (BU 3257/1-1). K. S. O. acknowledges support through an appointment to the Intelligence Community Postdoctoral Research Fellowship Program at the University of Maryland, administered by Oak Ridge Institute for Science and Education through an inter-agency agreement between the U.S. Department of Energy and the Office of the Director of National Intelligence. Figures were prepared using the PYTHON package MATPLOTLIB [47]. N. A. led the laboratory research and K. S. O. led the composition for this letter. N. A. redesigned the ensemble NV magnetometer developed by D. G. and D. B. B., performed the experiment, and data analysis. K. S. O. wrote the manuscript with the aid of N. A., J. T. O., and C. A. H., and performed additional data analysis. J. T. O. and C. A. H. aided in calibration measurements, simulations, data analysis, and letter composition. M. D. L., H. P. and R. L. W. conceived the present application of quantum logic enhanced sensing to NV-diamond AC magnetometry. D. H. provided the laboratory environment and technical guidance. R. L. W. supervised the project. All authors discussed the results and reviewed the manuscript.

\*Corresponding author: walsworth@umd.edu

- [1] K. Singh, S. Anand, A. Pocklington, J. T. Kemp, and H. Bernien, Dual-Element, Two-Dimensional Atom Array with Continuous-Mode Operation, *Phys. Rev. X* **12**, 011040 (2022).
- [2] C. D. Bruzewicz, J. Chiaverini, R. McConnell, and J. M. Sage, Trapped-ion quantum computing: Progress and challenges, *Appl. Phys. Rev.* **6**, 021314 (2019).
- [3] I. V. Inlek, C. Crocker, M. Lichtman, K. Sosnova, and C. Monroe, Multispecies Trapped-Ion Node for Quantum Networking, *Phys. Rev. Lett.* **118**, 250502 (2017).
- [4] F. Arute, K. Arya, R. Babbush, D. Bacon, J. C. Bardin, R. Barends, R. Biswas, S. Boixo, F. G. S. L. Brandao, D. A. Buell, B. Burkett, Y. Chen, Z. Chen, B. Chiaro, R. Collins *et al.*, Quantum supremacy using a programmable superconducting processor, *Nature (London)* **574**, 505 (2019).
- [5] P. O. Schmidt, T. Rosenband, C. Langer, W. M. Itano, J. C. Bergquist, and D. J. Wineland, Spectroscopy using quantum logic, *Science* **309**, 749 (2005).
- [6] T. Rosenband, P. O. Schmidt, D. B. Hume, W. M. Itano, T. M. Fortier, J. E. Stalnaker, K. Kim, S. A. Diddams, J. C. J. Koelemeij, J. C. Bergquist, and D. J. Wineland, Observation of the  $^1s_0 \rightarrow ^3p_0$  Clock Transition in  $^{27}\text{Al}^+$ , *Phys. Rev. Lett.* **98**, 220801 (2007).
- [7] D. B. Hume, T. Rosenband, and D. J. Wineland, High-Fidelity Adaptive Qubit Detection through Repetitive Quantum Nondemolition Measurements, *Phys. Rev. Lett.* **99**, 120502 (2007).
- [8] T. Rosenband, D. B. Hume, P. O. Schmidt, C. W. Chou, A. Brusch, L. Lorini, W. H. Oskay, R. E. Drullinger, T. M. Fortier, J. E. Stalnaker, S. A. Diddams, W. C. Swann, N. R. Newbury, W. M. Itano, D. J. Wineland, and J. C. Bergquist, Frequency ratio of  $\text{Al}^+$  and  $\text{Hg}^+$  single-ion optical clocks; metrology at the 17th decimal place, *Science* **319**, 1808 (2008).
- [9] J. F. Barry, J. M. Schloss, E. Bauch, M. J. Turner, C. A. Hart, L. M. Pham, and R. L. Walsworth, Sensitivity optimization for nv-diamond magnetometry, *Rev. Mod. Phys.* **92**, 015004 (2020).
- [10] D. A. Hopper, H. J. Shulevitz, and L. C. Bassett, Spin readout techniques of the nitrogen-vacancy center in diamond, *Micromachines* **9**, 437 (2018).
- [11] L. Jiang, J. S. Hodges, J. R. Maze, P. Maurer, J. M. Taylor, D. G. Cory, P. R. Hemmer, R. L. Walsworth, A. Yacoby, A. S. Zibrov, and M. D. Lukin, Repetitive readout of a single electronic spin via quantum logic with nuclear spin ancillae, *Science* **326**, 267 (2009).
- [12] P. Neumann, J. Beck, M. Steiner, F. Rempp, H. Fedder, P. R. Hemmer, J. Wrachtrup, and F. Jelezko, Single-shot readout of a single nuclear spin, *Science* **329**, 542 (2010).
- [13] I. Lovchinsky, A. O. Sushkov, E. Urbach, N. P. de Leon, S. Choi, K. De Greve, R. Evans, R. Gertner, E. Bersin, C. Müller, L. McGuinness, F. Jelezko, R. L. Walsworth, H. Park, and M. D. Lukin, Nuclear magnetic resonance detection and spectroscopy of single proteins using quantum logic, *Science* **351**, 836 (2016).
- [14] D. R. Glenn, D. B. Bucher, J. Lee, M. D. Lukin, H. Park, and R. L. Walsworth, High-resolution magnetic resonance spectroscopy using a solid-state spin sensor, *Nature (London)* **555**, 351 (2018).
- [15] E. V. Levine, M. J. Turner, P. Kehayias, C. A. Hart, N. Langellier, R. Trubko, D. R. Glenn, R. R. Fu, and R. L. Walsworth, Principles and techniques of the quantum diamond microscope, *Nanophotonics* **8**, 1945 (2019).
- [16] M. C. Marshall, R. Ebadi, C. Hart, M. J. Turner, M. J. H. Ku, D. F. Phillips, and R. L. Walsworth, High-Precision Mapping of Diamond Crystal Strain Using Quantum Interferometry, *Phys. Rev. Appl.* **17**, 024041 (2022).
- [17] S. Hsieh, P. Bhattacharyya, C. Zu, T. Mittiga, T. J. Smart, F. Machado, B. Kobrin, T. O. Höhn, N. Z. Rui, M. Kamrani, S. Chatterjee, S. Choi, M. Zaletel, V. V. Struzhkin, J. E. Moore, V. I. Levitas, R. Jeanloz, and N. Y. Yao, Imaging stress and magnetism at high pressures using a nanoscale quantum sensor, *Science* **366**, 1349 (2019).
- [18] D. M. Toyli, C. F. de las Casas, D. J. Christle, V. V. Dobrovitski, and D. D. Awschalom, Fluorescence thermometry enhanced by the quantum coherence of single spins in diamond, *Proc. Natl. Acad. Sci. U.S.A.* **110**, 8417 (2013).
- [19] P. Neumann, I. Jakobi, F. Dolde, C. Burk, R. Reuter, G. Waldherr, J. Honert, T. Wolf, A. Brunner, J. H. Shim, D. Suter, H. Sumiya, J. Isoya, and J. Wrachtrup, High-precision nanoscale temperature sensing using single defects in diamond, *Nano Lett.* **13**, 2738 (2013).
- [20] See Supplemental Material at <http://link.aps.org/supplemental/10.1103/PhysRevLett.131.100801> for additional details, which includes Refs. [11–14, 21–32].
- [21] A. M. Edmonds, C. A. Hart, M. J. Turner, P.-O. Colard, J. M. Schloss, K. S. Olsson, R. Trubko, M. L. Markham, A. Rathmill, B. Horne-Smith, W. Lew, A. Manickam, S. Bruce, P. G. Kaup, J. C. Russo, M. J. DiMario, J. T. South, J. T. Hansen, D. J. Twitchen, and R. L. Walsworth, Characterisation of CVD diamond with high concentrations of nitrogen for magnetic-field sensing applications, *Mater. Quantum Technol.* **1**, 025001 (2021).
- [22] H. Zhou, J. Choi, S. Choi, R. Landig, A. M. Douglas, J. Isoya, F. Jelezko, S. Onoda, H. Sumiya, P. Cappellaro, H. S. Knowles, H. Park, and M. D. Lukin, Quantum Metrology with Strongly Interacting Spin Systems, *Phys. Rev. X* **10**, 031003 (2020).
- [23] J. Choi, H. Zhou, H. S. Knowles, R. Landig, S. Choi, and M. D. Lukin, Robust Dynamic Hamiltonian Engineering of Many-Body Spin Systems, *Phys. Rev. X* **10**, 031002 (2020).
- [24] Y. Masuyama, K. Mizuno, H. Ozawa, H. Ishiwata, Y. Hatano, T. Ohshima, T. Iwasaki, and M. Hatano, Extending coherence time of macro-scale diamond magnetometer by dynamical decoupling with coplanar waveguide resonator, *Rev. Sci. Instrum.* **89**, 125007 (2018).
- [25] T. Wolf, P. Neumann, K. Nakamura, H. Sumiya, T. Ohshima, J. Isoya, and J. Wrachtrup, Subpicotesla Diamond Magnetometry, *Phys. Rev. X* **5**, 041001 (2015).
- [26] D. B. Bucher, D. R. Glenn, H. Park, M. D. Lukin, and R. L. Walsworth, Hyperpolarization-Enhanced NMR Spectroscopy with Femtomole Sensitivity using Quantum Defects in Diamond, *Phys. Rev. X* **10**, 021053 (2020).
- [27] N. Arunkumar, D. B. Bucher, M. J. Turner, P. TomHon, D. Glenn, S. Lehmkuhl, M. D. Lukin, H. Park, M. S. Rosen, T. Theis, and R. L. Walsworth, Micron-scale NV-NMR

- spectroscopy with signal amplification by reversible exchange, *PRX Quantum* **2**, 010305 (2021).
- [28] J. Holzgrafe, J. Beitner, D. Kara, H. S. Knowles, and M. Atatüre, Error corrected spin-state readout in a nanodiamond, *npj Quantum Inf.* **5**, 13 (2019).
- [29] V. V. Soshenko, S. V. Bolshedvorskii, O. Rubinas, V. N. Sorokin, A. N. Smolyaninov, V. V. Vorobyov, and A. V. Akimov, Nuclear Spin Gyroscope Based on the Nitrogen Vacancy Center in Diamond, *Phys. Rev. Lett.* **126**, 197702 (2021).
- [30] M. Ortner and L. G. Coliada Bandeira, Magpylib: A free PYTHON package for magnetic field computation, *SoftwareX* **11**, 100466 (2020).
- [31] A. Ajoy, B. Safvati, R. Nazaryan, J. Oon, B. Han, P. Raghavan, R. Nirodi, A. Aguilar, K. Liu, X. Cai *et al.*, Hyperpolarized relaxometry based nuclear  $T_1$  noise spectroscopy in diamond, *Nat. Commun.* **10**, 5160 (2019).
- [32] R. Wunderlich, R. Staacke, W. Knolle, B. Abel, J. Haase, and J. Meijer, Robust nuclear hyperpolarization driven by strongly coupled nitrogen vacancy centers, *J. Appl. Phys.* **130**, 104301 (2021).
- [33] A. Laraoui, F. Dolde, C. Burk, F. Reinhard, J. Wrachtrup, and C. A. Meriles, High-resolution correlation spectroscopy of  $^{13}\text{C}$  spins near a nitrogen-vacancy centre in diamond, *Nat. Commun.* **4**, 1651 (2013).
- [34] D. B. Bucher, D. P. L. Aude Craik, M. P. Backlund, M. J. Turner, O. Ben Dor, D. R. Glenn, and R. L. Walsworth, Quantum diamond spectrometer for nanoscale NMR and ESR spectroscopy, *Nat. Protoc.* **14**, 2707 (2019).
- [35] T. Staudacher, N. Raatz, S. Pezzagna, J. Meijer, F. Reinhard, C. A. Meriles, and J. Wrachtrup, Probing molecular dynamics at the nanoscale via an individual paramagnetic centre, *Nat. Commun.* **6**, 8527 (2015).
- [36] X. Kong, A. Stark, J. Du, L. P. McGuinness, and F. Jelezko, Towards Chemical Structure Resolution with Nanoscale Nuclear Magnetic Resonance Spectroscopy, *Phys. Rev. Appl.* **4**, 024004 (2015).
- [37] P. Kehayias, A. Jarmola, N. Mosavian, I. Fescenko, F. M. Benito, A. Laraoui, J. Smits, L. Bougas, D. Budker, A. Neumann, S. R. J. Brueck, and V. M. Acosta, Solution nuclear magnetic resonance spectroscopy on a nanostructured diamond chip, *Nat. Commun.* **8**, 188 (2017).
- [38] K. S. Liu, A. Henning, M. W. Heindl, R. D. Allert, J. D. Bartl, I. D. Sharp, R. Rizzato, and D. B. Bucher, Surface NMR using quantum sensors in diamond, *Proc. Natl. Acad. Sci. U.S.A.* **119**, e2111607119 (2022).
- [39] T. Gullion, D. B. Baker, and M. S. Conradi, New, compensated Carr-Purcell sequences, *J. Magn. Reson.* **89**, 479 (1990).
- [40] C. A. Ryan, J. S. Hodges, and D. G. Cory, Robust Decoupling Techniques to Extend Quantum Coherence in Diamond, *Phys. Rev. Lett.* **105**, 200402 (2010).
- [41] P. Siyushev, K. Xia, R. Reuter, M. Jamali, N. Zhao, N. Yang, C. Duan, N. Kukharchyk, A. D. Wieck, R. Kolesov, and J. Wrachtrup, Coherent properties of single rare-earth spin qubits, *Nat. Commun.* **5**, 3895 (2014).
- [42] A. Sajid, J. R. Reimers, and M. J. Ford, Defect states in hexagonal boron nitride: Assignments of observed properties and prediction of properties relevant to quantum computation, *Phys. Rev. B* **97**, 064101 (2018).
- [43] P. Udvarhelyi, G. m. H. Thiering, E. Londero, and A. Gali, Ab initio theory of the  $\text{n}_2\text{V}$  defect in diamond for quantum memory implementation, *Phys. Rev. B* **96**, 155211 (2017).
- [44] S. Castelletto and A. Boretti, Silicon carbide color centers for quantum applications, *J. Phys. Photonics* **2**, 22001 (2020).
- [45] A. Ruskuc, C.-J. Wu, J. Rochman, J. Choi, and A. Faraon, Nuclear spin-wave quantum register for a solid-state qubit, *Nature (London)* **602**, 408 (2022).
- [46] C. L. Degen, F. Reinhard, and P. Cappellaro, Quantum sensing, *Rev. Mod. Phys.* **89**, 035002 (2017).
- [47] Figures were prepared using MATPLOTLIB. J. D. Hunter, MATPLOTLIB: A 2d graphics environment, *Comput. Sci. Eng.* **9**, 90 (2007).